A Switchless Multiband Impedance Matching Technique Based on Multiresonant Circuits

Fabrício G. S. Silva, Robson N. de Lima, Raimundo Carlos S. Freire, and Calvin Plett

***Abstract*—In a number of applications, a matching network capable of providing specified impedances at different frequencies is necessary. In this brief, we present a novel technique for switchless multiband impedance matching networks based on multiresonant circuits. To illustrate this, simulation results of dual-band and triband networks are also presented. In addition, a dual-band impedance matching network has been implemented and evaluated. The dual-band impedance matching network presents two specified impedances, one at 433 MHz and the other at 915 MHz with 0.82 and 0.20 dB of insertion losses, respectively.**

***Index Terms*—Dual-band network, multiband amplifier, multiresonant circuits, switchless network, triband network.**

I. Introduction

IN THE WIRELESS world, there is a strong demand for multiband and multistandard RF transceivers aiming at flexibility and cost reduction. In the baseband interface, this flexibility is potentially obtainable via software, while in the RF front end, this feature is associated with the reconfigurability of its blocks, such as the low-noise amplifier, the oscillator, the mixer, and the power amplifier.

The multiband operation requires adjustable impedance matching networks, which can be possible by means of tunable [1] or switched [2], [3] circuit elements. However, these networks do not allow concurrent operation, which is necessary in applications involving harmonic manipulation, such as in high-efficiency amplifier design [4]. In addition, the use of solid-state switches imposes hard constraints on their control voltages, due to the large voltage swings at the control terminals, which may inadvertently lead to switch state changes [5]. Thus, a switchless impedance matching network can be a necessity, given that it allows concurrent operation and avoids the need for control signals in a multiband impedance matching network.

For switchless multiband network design, some techniques have been reported. However, these techniques rarely provide a complete solution in terms of lumped- or distributed-element circuits. In [6], a lumped filter design strategy is used to match only the real impedance loads. In [7] and [8], a dual-band impedance matching network for complex loads is proposed based on two-section shunt stubs whose design requires the numerical solution of nonlinear equations. In this context, we propose an impedance matching technique for multiband applications capable of working with lumped, distributed, and mixed networks. This technique allows analytical solution, synthesis of complex impedances, and harmonic manipulation. The idea consists of designing a switched network and replacing the switches with multiresonant circuits and then rearranging the circuit.

This brief is divided into four sections. In Section II, basic design principles are presented. In Section III, measurement results of a dual-band impedance network are presented, as well as the simulations results of a triband network. Finally, we summarize our major findings in Section IV.

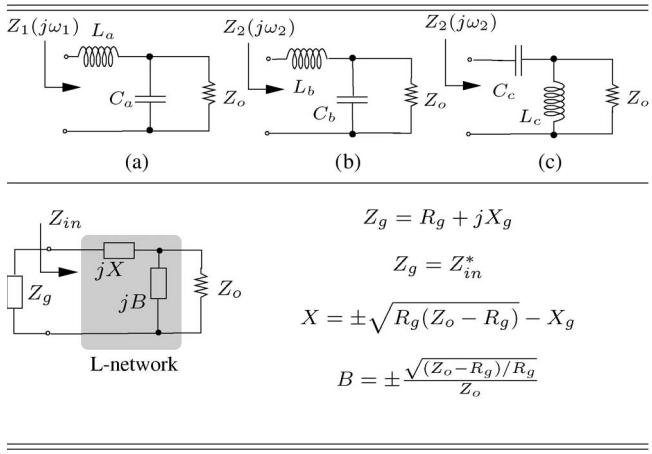

Fig. 1. L-networks for synthesis of impedances. (a) Z_1. (b) and (c) Z_2. Design equations of L-networks.

II. Basic Design Principles

To illustrate the method, consider the design of the L-impedance matching networks and their design equations, shown in Fig. 1. The first network [see Fig. 1(a)] presents an input impedance equal to Z_1 at ω_1 and the other two Z_2 at ω_2.

Assuming that our goal is to obtain a dual-band impedance matching network to synthesize the impedances Z_1 and Z_2, we can combine Fig. 1(a) and (b) L-networks by means of switches, as shown in Fig. 2(a). At ω_2, the impedance Z_2 is obtained when S_1 is closed and S_2 is open. When S_1 is open and S_2 is closed, the combination of impedance $j\omega_1 L_a$ and $1/j\omega_1 C_b 1/j\omega_1 C_x = 1/j\omega_1 C_a$ will result in Z_1 at ω_1.

Manuscript received October 3, 2012; revised December 28, 2012 and February 20, 2013; accepted April 17, 2013. Date of publication May 15, 2013; date of current version July 13, 2013. This work was supported in part by CNPq, by INCT/NAMITEC, and by CAPES. This brief was recommended by Associate Editor Prof. H. Barthelemy.

F. G. S. Silva is with the Department of Electrical and Electronical Technology (DTEE), Federal Institute of Technological Education of Bahia (IFBA), 40301-015 Salvador, Brazil.

R. N. de Lima is with the Department of Electrical Engineering, Federal University of Bahia (UFBA), 40110-909 Salvador, Brazil.

R. C. S. Freire is with the Department of Electrical Engineering, Federal University of Campina Grande (UFCG), 58109-900 Campina Grande, Brazil.

C. Plett is with the Department of Electronics, Carleton University, Ottawa, ON K1S 5B6, Canada.

Color versions of one or more of the figures in this brief are available online at http://ieeexplore.ieee.org.

Digital Object Identifier 10.1109/TCSII.2013.2261176

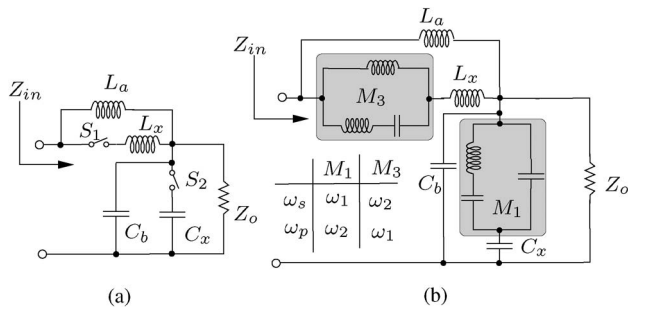

Fig. 2. Dual-band impedance matching networks.

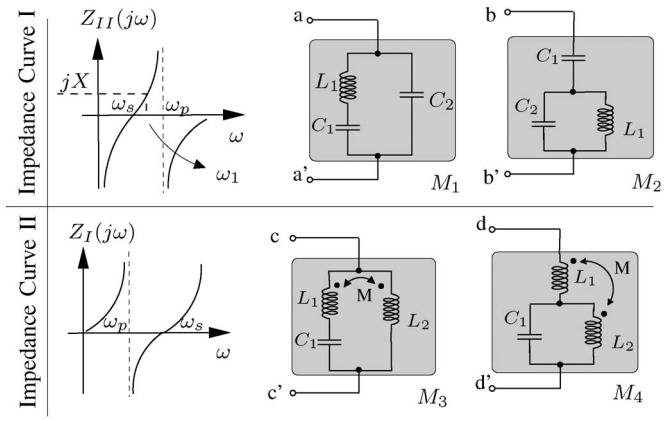

Fig. 3. Impedance characteristic of multiresonant circuits.

In our proposal, to transform the switched dual-band impedance matching network shown in Fig. 2(a) into a switchless one, we replace both the switches with the multiresonant circuits, whose impedance curves, presenting open and short circuits at different frequencies, create conditions to concurrently synthesize impedances. For instance, in Fig. 2(b), the switches S_1 and S_2 were replaced with the multiresonant circuits M_3 and M_1, respectively, so that the series resonance frequency of M_1 (ω_s) provides a short-circuit condition at ω_1 and the parallel resonance frequency (ω_p) provides an open-circuit one at ω_2, and as such can insert or remove, respectively, elements of the network.

In addition to circuits M_1 and M_3, a number of lossless multiresonant circuits, such as those shown in Fig. 3, can be obtained through Foster circuit synthesis techniques [9]. In Table I, the circuits M_1, M_2, M_3, and M_4 and their respective equations, interrelating their series (ω_s) and parallel (ω_p) resonance frequencies with capacitance and inductance, are presented [10].

In order to simplify the impedance network, it is also possible to explore other impedance regions of the multiresonant circuit to generate both capacitive and inductive reactances. For instance, as shown in Fig. 3, for $\omega_s < \omega_1 < \omega_p$, the impedance curve I presents an inductive behavior, and for $\omega_1 > \omega_p$ or $\omega_1 < \omega_s$, the impedance curve I presents a capacitive one. It is also possible to use a single resonant circuit (SRC_1), such as the series one, in order to compose an impedance network. To illustrate this, let us redesign the dual-band impedance matching network, making use of the circuits M_1 and SRC_1 to combine the L-networks in Fig. 1(a) and (c) into just one, according to the strategy illustrated in Fig. 4(a).

TABLE I
EQUATIONS OF THE LUMPED-ELEMENT MULTIRESONANT CIRCUITS

Circuit M_1	Circuit M_2
$\mathbf{Z_{aa'}(s)} = \frac{(1/C_2)(s^2+\omega_s^2)}{s(s^2+\omega_p^2)}$	$\mathbf{Z_{bb'}(s)} = \frac{s^2L_1(C_1+C_2)+1}{sC_1(s^2L_1C_2+1)}$
$\omega_p = \sqrt{\frac{C_1+C_2}{L_1C_1C_2}}$	$\omega_s = \sqrt{\frac{1}{L_1(C_1+C_2)}}$
$\omega_s = \sqrt{\frac{1}{L_1C_1}}$	$\omega_p = \sqrt{\frac{1}{L_1C_1}}$
Circuit M_3	**Circuit M_4**
$\mathbf{Z_{cc'}(s)} = L_{eq}\frac{s(s^2+\omega_s^2)}{s^2+\omega_p^2}$	$\mathbf{Z_{dd'}(s)} = L_{eq}\frac{s(s^2+\omega_s^2)}{(s^2+\omega_p^2)}$
$\omega_p = \sqrt{\frac{1}{C_1(L_1+L_2-2M)}}$	$L_{eq} = \left(\frac{L_2L_1-M^2}{L_2}\right)$, $\omega_p^2 = \frac{1}{L_2C_1}$
$\omega_s = \sqrt{\frac{L_2}{C_1(L_1L_2-M^2)}}$	$\omega_s = \sqrt{\frac{L_2+L_1+2M}{C_1(L_2L_1-M^2)}}$

where M is the mutual inductance.

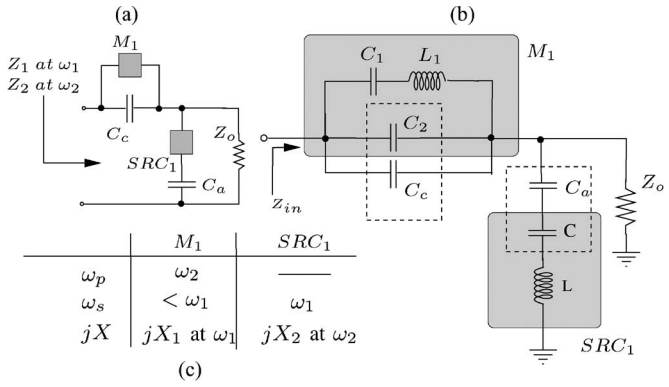

Fig. 4. (a) Design strategy. (b) Dual-band impedance matching network. (c) Operating conditions of circuits SRC_1 and M_1.

At ω_1, the multiresonant circuit M_1 generates an inductive reactance jX_1 at ω_1 for $\omega_1 > \omega_s$ such that the equivalent parallel impedance ($-j1/\omega_1C_cjX_1$) results in the impedance jX_{La}, and SRC_1 provides a short-circuit condition at $\omega_s = \omega_1$, thus obtaining the network in Fig. 1(a) which synthesizes Z_1. At ω_2, M_1 provides an open-circuit condition at $\omega_p = \omega_2$, and SRC_1 generates an inductive reactance jX_2 at ω_2 for $\omega_2 > \omega_s$ such that the series equivalent impedance ($-j1/\omega_2C_a + jX_2$) results in the impedance jX_{Lc}, obtaining the network in Fig. 1(c), which synthesizes Z_2. Fig. 4(c) summarizes the operating conditions of circuits SRC_1 and M_1.

Having designed the circuits M_1 and SRC_1 through the equations presented in Table II, one determines the capacitances resulting from the series combination C_a and C and the parallel one C_2 and C_c, as can be seen in Fig. 4(b), to finally obtain the dual-band network, as illustrated in Fig. 5.

A. Triband Impedance Matching Network

To further illustrate the proposed technique, let us consider the design of a triband mixed impedance matching network capable of synthesizing the impedances Z_1, Z_2, and Z_3 at ω_1, ω_2, and ω_3, where $\omega_3 > \omega_2 > \omega_1$. As the first step, the (a),

TABLE II
DESIGN EQUATIONS OF CIRCUITS M_1 AND SRC_1

SRC_1	M_1
$\mathbf{C} = \frac{\left(\frac{\omega_2}{\omega_1}\right)^2 - 1}{\mathbf{X_2}\omega_2}$	$\mathbf{C_2} = \frac{\omega_1^2 - \omega_s^2}{(\omega_2^2 - \omega_1^2)\mathbf{X_1}\omega_1}$
$\mathbf{L} = \frac{1}{\omega_1^2 \mathbf{C}}$	$\mathbf{C_1} = \mathbf{C_2}\left[\left(\frac{\omega_2}{\omega_s}\right)^2 - 1\right]$, $\mathbf{L_1} = \frac{1}{\omega_s^2 \mathbf{C_1}}$

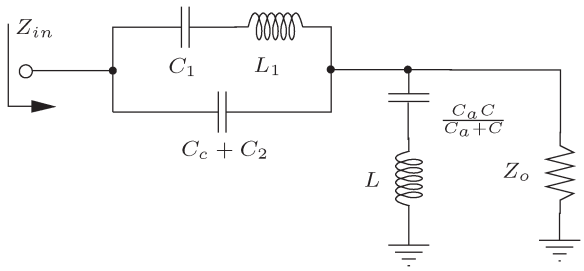

Fig. 5. Final dual-band impedance matching network using circuits M_1 and SRC_1.

TABLE III
L-NETWORKS FOR SYNTHESIS OF IMPEDANCES. (a) Z_1. (b) AND (c) Z_2. DESIGN EQUATIONS OF L-NETWORKS

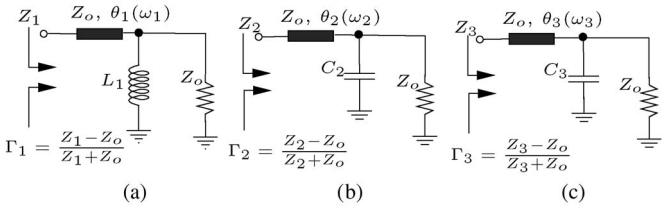

$$L_1 = \frac{Z_o\sqrt{1-|\Gamma_1|^2}}{2|\Gamma_1|\omega_1} \qquad C_i = \frac{2|\Gamma_i|}{Z_o\omega_i\sqrt{1-|\Gamma_i|^2}} \quad for\ i = 2,3$$

$$\theta_{11} = -\pi - \arctan\left(\frac{2\omega_1 L_1}{Z_o}\right) \qquad \theta_{11} = -\pi/2 - \arctan\left(\frac{Z_o\omega C_i}{2}\right)$$

$$\theta_1 = \frac{\theta_{11} - \angle\Gamma_1}{2} \qquad \theta_i(\omega_i) = \frac{\theta_{11} - \angle\Gamma_i}{2}$$

(1) (2)

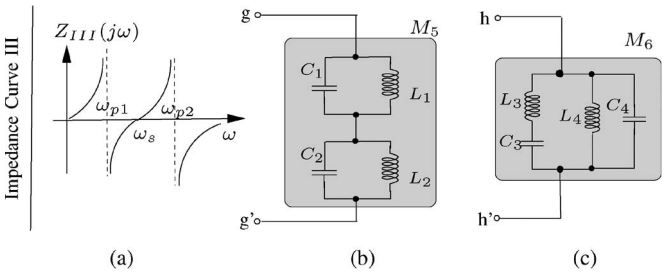

Fig. 6. (a) Impedance curve III. Multiresonant circuits (b) M_5 and (c) M_6.

(b), and (c) individual mixed L-networks shown in Table III are designed using equations (1) and (2) in Table III and then combined into a single one, using the multiresonant circuit M_5 [Fig. 6(b)], according to the impedance matching strategy shown in Fig. 7.

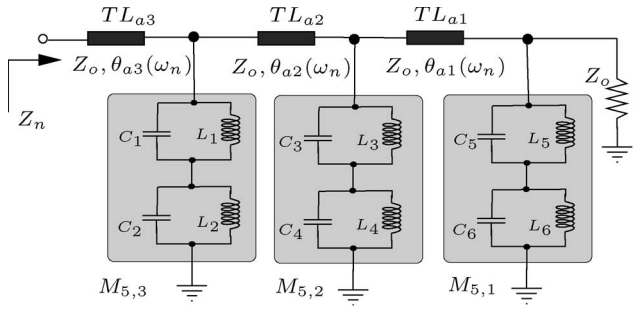

Fig. 7. Triband mixed impedance matching network using multiresonant circuit M_5.

TABLE IV
OPERATING CONDITIONS OF THE MULTIRESONANT CIRCUITS $M_{5,n}$

	$M_{5,3}$	$M_{5,2}$	$M_{5,1}$
ω_{p1}	ω_1	ω_1	ω_2
ω_{p2}	ω_2	ω_3	ω_3
ω_s	$\omega_1 < \omega_s < \omega_2$	$\omega_2 < \omega_s < \omega_3$	$\omega_2 < \omega_s < \omega_3$
jX	$-j/\omega_3 C_3$	$-j/\omega_2 C_2$	$j\omega_1 L_1$

For example, to synthesize Z_1, the multiresonant circuit $M_{5,1}$ generates an inductive reactance $j\omega_1 L_1$, and the circuits $M_{5,2}$ and $M_{5,3}$ provide open-circuit conditions at ω_1, such that the network in Table III(a) is obtained, which is formed by the inductor L_1 and three sections of transmission lines TL_{a3}, TL_{a2}, and TL_{a1}, whose total electrical length is given by $\theta_1(\omega_1) = \sum_{n=1}^{3} \theta_{an}(\omega_1)$, since the lines have the same characteristic impedance.

To synthesize Z_2, the circuits $M_{5,1}$ and $M_{5,3}$ provide open-circuit conditions at ω_2, and $M_{5,2}$ generates a capacitive reactance $-j/\omega_2 C_2$ at ω_2, thus generating the impedance network illustrated in Table III(b), whose series combination of transmission lines TL_{a2} and TL_{a3} produces a total electrical length equal to $\theta_2(\omega_2) = \sum_{n=2}^{3} \theta_{an}(\omega_2)$. The circuits $M_{5,1}$ and $M_{5,2}$ generate open-circuit conditions at ω_3, and $M_{5,3}$ generates a capacitive reactance $-j/\omega_3 C_3$ at ω_3, thus giving rise to the network shown in Table III(c), in which the transmission line TL_{a3} has an electrical length $\theta_3(\omega_3) = \theta_{a3}(\omega_3)$.Table IV summarizes the necessary conditions of $M_{5,n}$, for $n = 1, 2, 3$.

As can be seen in Table IV, the design of a triband matching network in Fig. 7 requires the following conditions: Each multiresonant circuit $M_{5,n}$, for $n = 1, 2, 3$, has to generate a reactance at one frequency and two open-circuit conditions at the two other frequencies. As a design example, consider the design of multiresonant circuit $M_{5,3}$ using the following assumptions: $\omega_{p1} = \omega_1$ and $\omega_{p2} = \omega_2$ in order to generate the open-circuit conditions, $jX = -j/\omega_3 C_3$ at ω_3, and the series resonance frequency domain is limited by (ω_1, ω_2), i.e., $\omega_1 < \omega_s < \omega_2$, as shown in Table IV. Then, considering $\{\omega_s, \omega_1, \omega_2, -1/\omega_3 C_3, \omega_3\}$ as the input variables, we determine the inductances L_1 and L_2 and the capacitances C_1 and C_2 of circuit $M_{5,3}$ using the equations in Table V.

Another mixed triband impedance matching network can be obtained by using the multiresonant circuit M_6 [Fig. 6(c)], as shown in Fig. 8, whose element values are obtained from the equations derived from the equivalence with the multiresonant circuit M_5 (Table V), i.e., the capacitances and

TABLE V
EQUATIONS OF MULTIRESONANT CIRCUITS $M_{5,3}$ AND $M_{6,3}$

Circuit $M_{5,3}$	Circuit $M_{6,3}$
$\mathbf{n} = \frac{\omega_s^2-\omega_2^2}{\omega_1^2-\omega_2^2}$	$\mathbf{L_7} = \frac{\mathbf{L_1L_2(L1+L_2)(C_1+C_2)^2}}{\mathbf{(L_1C_1-L_2C_2)^2}}$
$\mathbf{C_2} = \frac{\omega_3(\omega_s^2-\omega_3^2)}{\mathbf{n}(\omega_1^2-\omega_3^2)(\omega_2^2-\omega_3^2)\mathbf{X}}$	$\mathbf{L_8 = L_1 + L_2}$
$\mathbf{C_1} = \frac{\mathbf{nC_2}}{\mathbf{1-n}}$	$\mathbf{C_8} = \frac{\mathbf{C_1C_2}}{\mathbf{C_1+C_2}}$
$\mathbf{L_1} = \frac{1}{\omega_1^2\mathbf{C_1}}$, $\mathbf{L_2} = \frac{1}{\omega_2^2\mathbf{C_2}}$	$\mathbf{C_7} = \frac{\mathbf{(L_1C_1-L_2C_2)^2}}{\mathbf{(C_1+C_2)(L_1+L_2)^2}}$

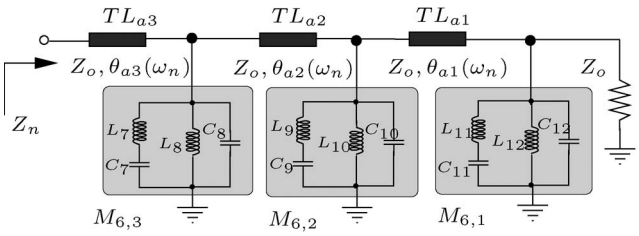

Fig. 8. Triband mixed impedance matching network using multiresonant circuit M_6.

inductances $\{C_7, C_8, L_7, L_8\}$ of the circuit $M_{6,3}$ are equivalent to $\{C_1, C_2, L_1, L_2\}$ of circuit $M_{5,3}$.

This new multiband circuit (Fig. 8) can facilitate the transformation of the mixed network into a complete distributed network using the equivalence between transmission lines and lumped elements [11]. However, in a lumped implementation, the network M_5 is more appropriate given that some parasitic capacitance in shunt with the inductor can be absorbed into the circuit, whereas in the circuit M_6, the parasitic capacitance of the inductor in the LC series arm cannot be so readily absorbed.

III. MEASUREMENT AND SIMULATION RESULTS

To evaluate the performance of the proposed methodology, let us consider the synthesis of a dual-band impedance network, whose optimum impedances are $Z_1 = 36.46 - j3.680\ \Omega$ and $Z_2 = 35.34 + j10.91\ \Omega$ at 433 and 915 MHz, respectively.

The L-networks illustrated in Fig. 9(a) and (b) are individually designed and then combined through the multiresonant circuit such that a switchless dual-band network could be obtained, as shown in Fig. 9(c).

The dual-band network [Fig. 9(c)] was mounted on an FR4 substrate (relative dielectric constant of 4.40 and thickness of 900 μm) using lumped surface-mount devices (SMDs) from AVX and Johanson Technologies manufacturers. Fig. 9(d) shows a photograph of this network.

The Agilent network analyzer E5071C, under the SOLT calibration method, has been used to measure the S-parameters of the circuit at 433 and 915 MHz. According to the results presented in Fig. 10, the measured reflection coefficients $\Gamma_{\text{in},m}$, with respect to the target impedances, are smaller than -15.0 dB (0.177), and the insertion losses are 0.20 dB at 433 MHz and 0.82 dB at 915 MHz, which show the potential of the proposed technique.

In order to compare the performance of this dual-band impedance network to a switched dual-band one [Fig. 2(a)],

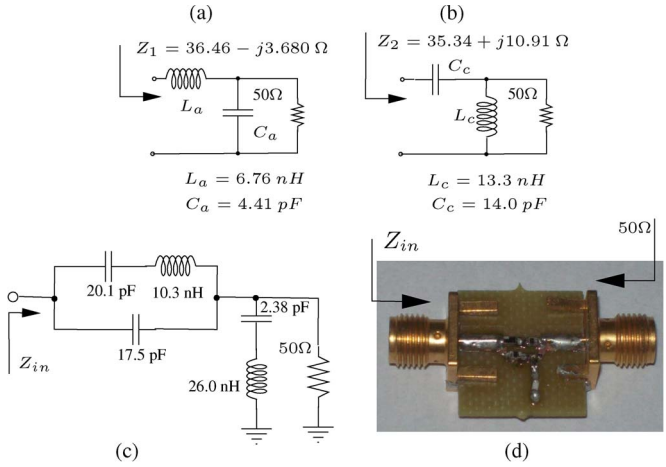

Fig. 9. (a) and (b) L-networks to synthesize the desired impedances. (c) Dual-band matching network. (d) Photograph of the dual-band network.

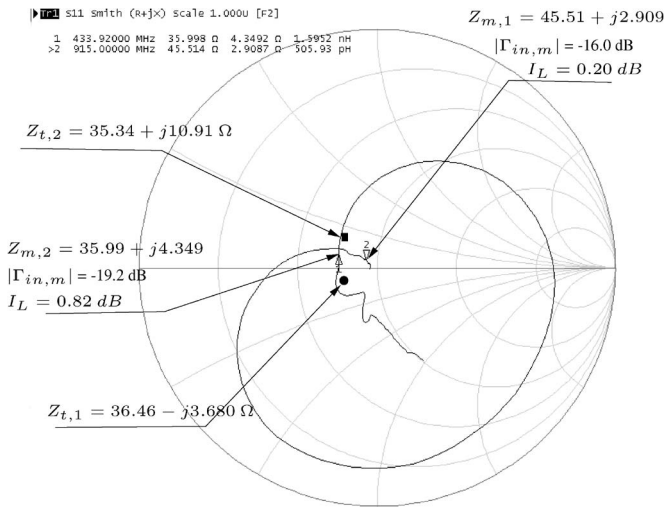

Fig. 10. Target and measured impedances presented in Smith Cart, where Z_t is a target impedance, Z_m is the measured impedance, and $\Gamma_{\text{in},m}$ is the measured reflection coefficient.

TABLE VI
RESULTS CONSIDERING DEVICES FROM AVX COMPONENTS AND JOHANSON TECHNOLOGIES AND PHEMT SWITCHES

Frequencies	433 MHz	915 MHz
Target Impedances ($Z_t(\Omega)$)	36.46 - j3.680	35.34 + j10.91
Simulation Results with Multiresonant Circuits		
$Z_{sim}(\Omega)$	42.53 - j4.264	37.67 + j12.78
$\lvert\Gamma_{in}\rvert(dB)$	-22.2	-27.8
$I_L(dB)$	0.51	0.03
Simulation Results with Switches		
$Z_{sim}(\Omega)$	39.56 - j4.387	38.46 + j12.86
$\lvert\Gamma_{in}\rvert(dB)$	-27.6	-26.0
$I_L(dB)$	0.02	0.12

we considered the switches implemented with pHEMT and modeled by a simple capacitor in the OFF state ($C_{\text{OFF}} = 160fF$) and a resistor in the ON state ($R_{\text{ON}} = 1.4\ \Omega$) [12]. The simulation results are shown in Table VI. As can be seen, the

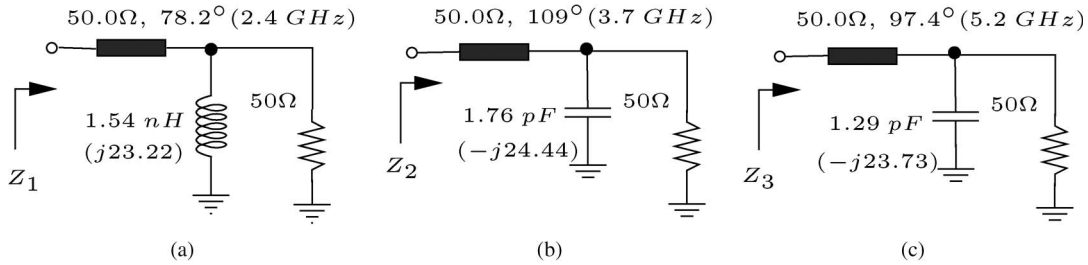

Fig. 11. Networks for synthesis of (a) Z_1, (b) Z_2, and (c) Z_3.

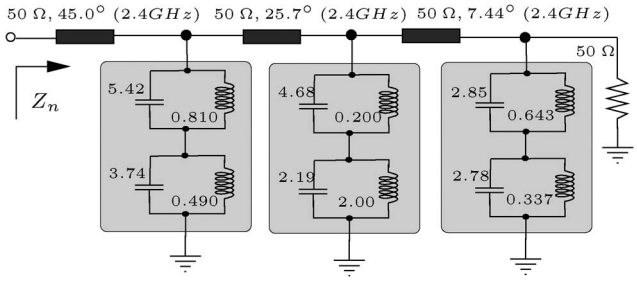

Fig. 12. Triband impedance matching network. Capacitance in picofarads. Inductance in nanohenrys.

TABLE VII
POSTLAYOUT SIMULATION RESULTS CONSIDERING DUROID 5880 SUBSTRATE AND DEVICES FROM MURATA COMPONENTS

Freq.	2.4 GHz	3.7 GHz	5.2 GHz
$Z_t(\Omega)$	151.5 - j158.0	271.2 + j89.32	93.50 + j137.7
Simulation Results			
$Z_{sim}(\Omega)$	162.2 - j123.7	270.9 + j71.19	87.88 + j119.6
$\lvert\Gamma_{in}\rvert(dB)$	-18.9	-29.5	-19.7
$I_L(dB)$	0.62	0.68	1.06

insertion losses are not significantly different, which illustrates the potential of the proposed technique.

A mixed triband matching network was designed and evaluated through postlayout simulations. Accordingly, the L-networks, illustrated in Fig. 11, were combined using the multiresonant circuit M_5 to synthesize the impedances $Z_1 = 151.5 - j158.0\,\Omega$, $Z_2 = 271.2 + j89.32\,\Omega$, and $Z_3 = 93.50 + j137.7\,\Omega$ at frequencies of 2.4, 3.7, and 5.2 GHz, respectively, thus resulting in the network shown in Fig. 12.

This triband network has been evaluated by postlayout simulation, assuming a realization on ROGERS RT/Duroid 5880 substrate and using lumped SMD from Murata Components manufacturers. According to the results, the magnitudes of the reflection coefficients at 2.4, 3.7, and 5.2 GHz are less than -18.0 dB, and the maximum insertion loss is 1.06 dB, as shown in Table VII. These results corroborate the potential of the proposed impedance matching technique for mixed networks as well.

IV. CONCLUSION

In this brief, we have presented a novel design technique for multiband impedance matching networks based on multiresonant circuits, which are capable of providing short- and open-circuit conditions at specified frequencies, thus enabling and disabling capacitors and inductors to form a multiband impedance matching network. To validate this technique, dual-band and triband impedance networks have been designed. The measurement results of the dual-band lumped network for operation at 433- and 915-MHz bands show that the reflection coefficients, with respect to the target impedances, are smaller than -15.0 dB (0.177) and the insertion losses are equal to 0.20 dB at 433 MHz and 0.82 at 915 MHz. The insertion loss of less than 1.1 dB and the magnitudes of the reflection coefficients less than -18.0 dB for the triband mixed network, operating at 2.4, 3.7, and 5.2 GHz, reveal that the proposed technique is potentially usable in the design of multiband impedance matching networks.

ACKNOWLEDGMENT

The authors would like to thank SENAI/CIMATEC for the printed circuit board fabrication.

REFERENCES

[1] J. L. Brown and N. M. Neihart, "An analytical study of a magnetically tuned matching network," in *Proc. IEEE ISCAS*, 2012, pp. 1979–1982.
[2] P. Sjöblom and H. Sjöland, "Measured CMOS switched high-quality capacitors in a reconfigurable matching network," *IEEE Trans. Circuits Syst. II, Exp. Briefs*, vol. 54, no. 10, pp. 858–862, Oct. 2007.
[3] X. Yu and N. M. Neihart, "Integrated multi-tap transformer for reconfigurable multimode matching networks," in *Proc. IEEE Int. Symp. Circuits Syst.*, 2011, pp. 1395–1398.
[4] P. Colantonio, F. Giannini, R. Giofre, and L. Piazzon, "A design technique for concurrent dual-band harmonic tuned power amplifier," *IEEE Trans. Microw. Theory Tech.*, vol. 56, no. 11, pp. 2545–2555, Nov. 2008.
[5] M. B. Shifrin, P. J. Katzin, and Y. Ayasli, "Monolithic FET structures for high-power control component applications," *IEEE Trans. Microw. Theory Tech.*, vol. 37, no. 12, pp. 2134–2141, Dec. 1989.
[6] Y. Takayama, K. Uchida, T. Fujita, and K. Maenaka, "Microwave dual-band power amplifiers using two-frequency matching," *Electron. Commun. Jpn.*, vol. 89, no. 5, pp. 17–24, May 2006.
[7] M. Chuang, "Dual-band impedance transformer using two-section shunt stubs," *IEEE Trans. Microw. Theory Tech.*, vol. 58, no. 5, pp. 1257–1263, May 2010.
[8] Y. Wu, Y. Liu, and S. Li, "A dual frequency transformer for complex impedances with two unequal sections," *IEEE Microw. Wireless Compon. Lett.*, vol. 19, no. 2, pp. 77–79, Feb. 2009.
[9] R. M. Foster, "A reactance theorem," *Bell System Technical Journal*, vol. 302, no. 3, pp. 259–267, Apr. 1924.
[10] F. G. S. Silva, R. N. de Lima, S. M. Nascimento, and R. C. S. Freire, "A design methodology for concurrent impedance matching networks based on multiresonant circuits," in *Proc. IEEE 9th Int. NEWCAS*, 2011, pp. 386–389.
[11] F. G. S. Silva, R. N. de Lima, S. M. Nascimento, and R. C. S. Freire, "A concurrent dualband distributed impedance-matching network," in *Proc. 24th Symp. Integr. Circuits Syst. Des.*, New York, NY, USA, 2011, pp. 11–16.
[12] P. Hindle, "The sate of RF/microwave switch devices," *Microw. J.*, vol. 53, no. 11, pp. 20–36, Nov. 2010.